CHEMISTRY OF MATERIALS
Review

Chem. Mater. **2010,** *22,* 3569–3579 3569
DOI:10.1021/cm1004592

Transparent Conducting Oxides in the ZnO-In_2O_3-SnO_2 System

Cathleen A. Hoel,[†] Thomas O. Mason,[‡] Jean-François Gaillard,[§] and Kenneth R. Poeppelmeier*,[†]

[†]*Department of Chemistry, Northwestern University, 2145 Sheridan Road, Evanston, Illinois 60208-3113,* [‡]*Department of Materials Science and Engineering, Northwestern University, 2220 Campus Drive, Evanston, Illinois 60208-3108, and* [§]*Department of Civil and Environmental Engineering, Northwestern University, 2145 Sheridan Road, Evanston, Illinois 60208-3113*

Received February 12, 2010. Revised Manuscript Received April 22, 2010

Zinc-indium-tin oxide (ZITO) is a potential replacement for the currently used tin-doped indium oxide (ITO) as a transparent conducting oxide (TCO) for optoelectronic devices. At the present time ITO is the material of choice for the TCO layer, but the increasing cost of indium metal and the advent of new technologies will require alternative TCOs. Over the past 15 years, bulk and thin film studies have been amassed that report the electrical and optical properties of various ZITO compositions. This review will examine the reported data and demonstrate that the bulk subsolidus phase diagram can act as a guide to understanding the numerous and varied results reported for thin films.

Introduction

Transparent Conducting Oxides (TCOs). Transparent conducting oxides are degenerately doped semiconductor oxides that are transparent to visible light. These simultaneous properties enable numerous applications, such as flat-panel displays, photovoltaic devices, and light-emitting diodes (LED).[1−4] Popular TCOs include In_2O_3:Sn (ITO), SnO_2:F, and ZnO:Al. ITO dominates the market in high-end electronics with conductivities reaching 10,000 S/cm.[5−7] ITO is the most common usage of indium, accounting for 82% of indium metal consumed in the United States.[8] Indium, however, is a scarce metal. The worldwide production in the year 2005 was 500 t, which composes approximately 8% of the total estimated reserve base. Although there is a general lack of infrastructure needed to recycle significant quantities of the metal, recycling indium will become increasingly important. The recent increase in demand for indium coupled with its natural scarcity is reflected in its market value.[9,10] The price of indium metal was steady at $72/kg before 1960 when its major usage was in solder alloys. After 1970 the price fluctuated erratically and eventually rose to $946/kg by 2005 followed by a decline to $685/kg for 2008. Because of the high cost and low supply of indium, researchers are searching for indium-free TCOs.

For the last 15 years, the cosubstitution chemistry of ZnO and SnO_2 (two relatively inexpensive materials) in In_2O_3 has been explored.[11,12] Great progress has been made toward understanding the relationship between the bulk equilibrium structure and the electrical and optical properties. Most materials, however, are utilized in thin film form in devices and transparent conductors are no exception. Numerous films in the ZnO-In_2O_3-SnO_2 (ZITO) system have been grown and their electronic properties have been examined as a function of composition and deposition conditions. This review will organize and summarize the previous work that has been done in the ZITO system for thin films and compare these results to bulk studies with the goal to provide clear directions for further work.

Electronic Properties of TCOs. The unique simultaneity of electrical conduction and visible transparency stems from specific structural motifs. TCOs satisfy three conditions as outlined by Hamberg and Granqvist.[13]

(1) The oxide must have a band gap of at least 3.1 eV to transmit at least 85% visible light in thin film form.

(2) The metal oxide must be susceptible to degenerate doping so that the pure oxide can transition from a transparent oxide semiconductor to a metallic conductor. When carrier densities become greater than 2.6×10^{21} cm^{-3}, however, the TCO exhibits plasma frequencies that move from absorbing infrared wavelengths to visible light.[14] These absorptions in the visible range reduce the transparency of the TCO.

(3) The metal cations typically have an $(n-1)d^{10}ns^0$ (n = 4, 5) electronic configuration, such as Zn^{2+}, Ga^{3+}, Cd^{2+}, In^{3+}, and Sn^{4+}. The carriers reside in the conduction band bottom, which is composed of the ns^0 orbitals, and owing to their spherical symmetry, these diffuse orbitals overlap to create bands allowing for high electron mobilities. The filled d levels prevent d-d electronic transitions from occurring in the visible region of the spectrum.[15] Conditions 1 and 2 have no exceptions because they define the optical and electrical

*To whom correspondence should be addressed. E-mail: krp@northwestern.edu.

© 2010 American Chemical Society
Published on Web 05/13/2010

properties of the TCO. Some TCOs, however, have been found that do not meet condition 3. For example, mayenite is a TCO which has a $12CaO\cdot7Al_2O_3$ cage structure.[16] The Ca^{2+} and Al^{3+} cations are low Z metals with no d electrons. Non-d^{10} cations, including Mo^{6+}, Sc^{3+}, and Mg^{2+}, can also be used as dopants[17,18] or one component of a layered[19] or spinel[20] TCO. It should be noted that transition metal cations with partially filled d-orbitals are, in general, avoided to prevent d-d transitions.

Structures of the End Points: ZnO, In_2O_3, and SnO_2. To better understand the equilibrium phases that form in the ZITO multicomponent system, we first briefly review the three end points. ZnO takes the form of wurtzite, which is a tetrahedral structure where zinc is coordinated by four oxygen atoms and oxygen is coordinated by four zinc atoms.[21] The structure consists of a hexagonal close packing of oxygen anions with zinc cations filling half of the tetrahedral holes, all of which exhibit the same orientation.[22] In_2O_3 adopts the bixbyite structure, which is also known as the C-type modification of the rare-earth sesquioxides.[23] Bixbyite is described as a fluorite-type structure with one-quarter of the anions "missing" in an ordered fashion. The cations reside at the body-center of a cube with anions occupying the corners. The two "missing" anions are located either across the body-diagonal of the cube (b site) or the face-center of the cube (d site). The designations of the two cation sites are derived from the Wyckoff positions, 8b and 24d, respectively. Each oxygen is then coordinated by four indium cations. SnO_2 crystallizes in the rutile structure type where tin is coordinated by six oxygen atoms and oxygen is coordinated by three tin atoms.[24] Rutile is described by a hexagonal close packing of the anions with half of the octahedral holes filled by the cations.

ITO Background. It is necessary to be familiar with ITO, the current benchmark TCO before exploring alternate systems. At equilibrium and in the bulk the solubility of SnO_2 in In_2O_3 has been reported to be about 6% (cation basis),[25,26] but precise synchrotron diffraction studies revealed a solubility of 1−4% depending on the temperature.[27] Solubility levels of thin films, however, have reported up to 39% Sn doping In_2O_3.[28,29] Although powder X-ray diffraction (XRD) did not reveal the presence of SnO_2 crystals, the extended X-ray absorption fine structure (EXAFS) at the Sn K edge showed that Sn was in a similar coordination environment as in SnO_2 and demonstrated the formation of SnO_2-type environments at high Sn concentrations.[28,29] Reported results of ITO films show that the highest conductivities occur at 6−9% Sn.[5,7]

Indium oxide is an n-type semiconductor that is self-doped by oxygen vacancies, $V_O^{\cdot\cdot}$.[30,31] The conductivity of In_2O_3 ranges from 10^{-4} to 10^3 S/cm[32−36] depending on the oxygen partial pressure such that oxidizing atmospheres yield low conductivities and, conversely, reducing atmospheres give high conductivities.[32,34,35,37] When In_2O_3 is doped to make ITO, $Sn_{In}^{\cdot}$ becomes the primary donor.[15,30] ITO, however, exhibits the same type of

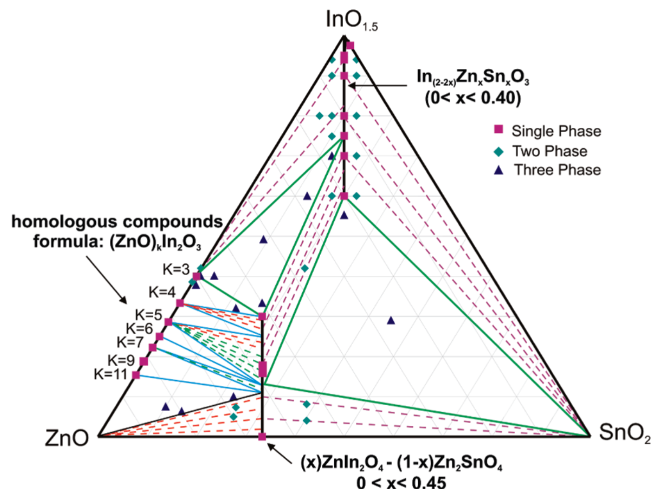

Figure 1. Subsolidus phase diagram of $ZnO-In_2O_3-SnO_2$ at 1275 °C and 1 atm. Reprinted with permission from Harvey et al.[12]. Copyright 2008 Wiley-Blackwell. Single phase points are denoted by a square, two phase points are denoted by a diamond, and three phase points are denoted by a triangle.

conductivity dependence on oxygen partial pressure as In_2O_3.[38,39] Frank and Köstlin[5] proposed the existence of a neutral reducible associate between tin donors and oxygen interstitials now known as a Frank−Köstlin associate, $(2Sn_{In}^{\cdot}O_i'')^x$, that is, the SnO_2 reacts with the In_2O_3 by incorporation of the compensating equivalents of oxygen. This cluster traps Sn donor electrons, but a reducing treatment will remove the oxygen interstitials and release the carrier. Likewise, an oxidizing anneal will insert oxygen interstitials and trap the carriers. This associate is consistent with the conductivity dependence of ITO on the atmospheric conditions and a variety of conductivity, neutron diffraction, and theoretical studies support its existence.[5,27,40,41]

$ZnO-In_2O_3-SnO_2$ or ZITO System. ZITO was first reported in 1995 by Phillips et al.[42] where thin films were grown from polycrystalline oxide targets by pulsed laser deposition. The target compositions were $Zn_xIn_{2-y}Sn_yO_{3+x+0.5y-\delta}$ ($1.4 \le x \le 4$ and $0 \le y \le 0.4$). The targets were single-phase for the compositions $Zn_3In_{2-y}Sn_yO_{6-\delta}$ ($0 \le y \le 0.15$), which corresponds to Sn-doped $Zn_3In_2O_6$. Phillips et al. explored the conductivity dependence of the [Zn]/[In] ratio for each film. The targets had [Zn]/[In] ratios ranging from 0.8 to 2.2 while the [Sn]/[In] ratio was kept in the range 0.05 to 0.18. The composition of the films contained less zinc than the targets, such that the [Zn]/[In] ratios ranged from 0.25 to 1.6. The [Sn]/[In] film ratios were presumed to be similar to the target. Every film was amorphous, with the exception of the film corresponding to [Zn]/[In] = 0.25, which showed bixbyite domains by XRD. The conductivity of the amorphous films decreased as the [Zn]/[In] ratio increased. The film conductivity peaked for the composition $ZnIn_{1.7}Sn_{0.3}O_{3.65-\delta}$ at 2600 S/cm.

Bulk Equilibrium ZITO. In 1997, Palmer et al.[11,43,44] started to explore the subsolidus phase diagram for the $ZnO-In_2O_3-SnO_2$ system. The bulk equilibrium ZITO phase diagram (Figure 1) was completed in 2008 by Harvey et al.[12] The subsolidus phase diagram of ZITO

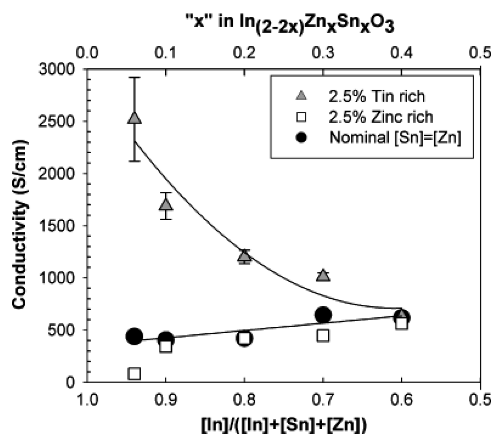

Figure 2. Conductivity dependence of $In_{2-2x}Sn_xZn_xO_3$ on relative ratio of [Sn]:[Zn]. Reprinted with permission from Harvey et al.[44]. Copyright 2008 Wiley-Blackwell. Lines are drawn to guide the eye.

shows no unique ternary compounds, but there are two solid solutions of interest. One solid solution results from the cosubstitution of Zn and Sn into In_2O_3, which gives the general formula $In_{2-2x}Zn_xSn_xO_3$ ($x \leq 0.4$).[44] Pellets of the bulk powder prepared along this solid solution line have conductivities close to those of ITO.[44-47] Although the samples were prepared with equivalents of Zn and Sn, that is, no net doping, n-type conduction persisted. The doping limits of $In_{2-2x}Zn_xSn_xO_3$ were explored by preparing pellets with a slight excess of Zn or Sn.[45] Pellets of $In_{2-2x}Zn_xSn_xO_3$ with a Sn-excess ([Sn]/[Zn] > 1) showed n-type conduction reaching up to 4000 S/cm. Specimens of $In_{2-2x}Sn_xZn_xO_3$ with a Zn-excess ([Sn]/[Zn] < 1) showed n-type conduction of ~500 S/cm. The conductivities as a function of composition are plotted in Figure 2. Ambrosini et al.[48] examined Zn as an acceptor for a series of Zn-excess samples (0 < [Zn] − [Sn] < 4%). $In_{1.64}Sn_{0.16}Zn_{0.2}O_{3-\delta}$ (4% Zn excess) was annealed under high oxygen pressure to trap donor electrons, which caused the carrier concentration to drop from 10^{20} cm^{-3} to 10^{18} cm^{-3}. The conductivity temperature dependence indicated a transition from a degenerate to nondegenerate semiconductor after the oxygen anneal. The transition from n-type to p-type conductivity, however, was not observed despite the electron trapping and excess Zn acceptors. In fact, p-type conduction has not been observed for an In-based TCO, with the exception of $CuInO_2$.[49] Several defects have been proposed to account for this conduction behavior including Frank-Köstlin-type $(2Zn_{In}{'}V_O{^{\bullet\bullet}})^x$ associates[45,48] and an inherent Sn-excess at equilibrium.[45]

The ZITO system exhibits a second solid solution, In_2O_3-substituted Zn_2SnO_4, which is described by the general formula $Zn_{2-x}Sn_{1-x}In_{2x}O_4$ ($x \leq 0.45$).[43] Zn_2SnO_4 is an inverse spinel and two In^{3+} atoms "reverse cosubstitute" for Zn^{2+}/Sn^{4+} pairs. The Zn_2SnO_4 spinel showed poor electrical conduction and continued to do so upon In substitution.[43] The highest measurable conductivity for the bulk spinel reported is 3 S/cm, and it occurred at the upper indium substitution limit ($x = 0.45$) after a strong reduction treatment.[43] In prior work, one of the authors showed that as-prepared ZITO spinels had orders of magnitude lower conductivity than the corresponding CITO spinels (Cd-In-Sn-O).[50] Noting that Zn_2SnO_4 is an inverse spinel, it was argued that Zn is not an effective TCO cation neither in octahedral coordination nor in tetrahedral coordination (vis-à-vis Cd, In, or Sn). In particular, the tetrahedral Zn−Zn distance (for orbital overlap) is approximately 20% longer than it is in the well-known zinc oxide TCO. The precise origin for the low conductivity, whether attributable to low mobilities, low carrier contents, or both, remains to be resolved. In addition, the underlying defect mechanism(s) remain uncertain. Reduction treatments increase the conductivity, which has been attributed to the contribution of oxygen vacancy donors, but confirmation is lacking.

Along the ZnO-In_2O_3 binary exists the homologous series $(ZnO)_kIn_2O_3$ (k = 2−7, 9, 11, 13, 15, 20). At 1275 °C, the phases at k = 3, 4, 5, 7, 9, and 11 form as evident in Figure 1. The phases for k = 2, 6, 8, 15, and 20 form at temperatures up to 1550 °C.[12,51-53] The first reported ZITO films, grown by Phillips et al.,[42] had compositions that correspond to $k \approx 2, 3$. The structure is composed of alternating octahedral InO_2^- layers and wurtzite-like $InZn_kO_{k+2}^+$ slabs. The indium and zinc were determined by Reitveld refinement to be disordered in the $InZn_kO_{k+2}^+$ section of $Zn_3In_2O_6$.[54] TEM of $Zn_{15}In_2O_{18}$, however, showed modulation of the In atoms to form a zigzag pattern in the $InZn_kO_{k+2}^+$ layer.[55] The degree of order and modulation between the In and Zn and its dependence on the synthesis is not known for each k-phase. Detailed descriptions of the proposed structures are given in references 51,54−60. The relationship between the structure and electronic properties is also not well understood. The conductivities of bulk $(ZnO)_kIn_2O_3$ (k = 3−7, 11) increased as k decreased from 1 S/cm for $Zn_{11}In_2O_{14}$ to 270 S/cm for $Zn_3In_2O_6$.[51] As will be discussed later, thin film conductivities can be over 1000 S/cm. Much like the $In_{2-2x}Sn_xZn_xO_3$ solid solution, the $(ZnO)_kIn_2O_3$ series is conductive without external dopants such as Sn. Sn-doping marginally increased the conductivities.[61-63] Because the $(ZnO)_kIn_2O_3$ structure is composed of distinct layers, the conductivity was presumed to scale linearly with k, but this behavior was not observed. The order and disorder exhibited by the indium and zinc site occupancies in the $InZn_kO_{k+2}^+$ slabs may contribute to the carrier generation mechanism, but this source has not been examined thoroughly yet. The conductivities improved after a reduction treatment, so the source of conductivity has been attributed to oxygen vacancies in the past, but this defect is not consistent with the observed relationship between the conductivity and partial oxygen pressure.[51] The non-linear trend between the carrier concentration and k value suggests a defect other than oxygen vacancies plays a significant role for electron generation.[51] Owing to the complexity of the crystal structure and its variations for each value of k, the carrier source remains elusive. All other regions in the ZnO-In_2O_3-SnO_2 system exhibit mixtures of the aforementioned phases at bulk equilibrium.

The ZnO-In_2O_3-SnO_2 subsolidus phase diagram does not show the known binary phase $In_4Sn_3O_{12}$. The ZITO

Table 1. Highest Performing ZITO Film from Each Study[a]

normalized composition	σ (S·cm^{-1})	μ (cm^2 V^{-1} s^{-1})	n (× 10^{20} cm^{-3})	phases (deposition)	reference
$Zn_{0.33}In_{0.57}Sn_{0.1}O_{1.5}$	2630	NR	NR	amorphous (*a450, s*)	Phillips et al.[139] 1995
$Zn_{0.5}In_{0.49}Sn_{0.01}O_{1.25}$	3333	25	4	NR (*aRT, s*)	Minami et al.[66] 1998
$Zn_{0.35}In_{0.52}Sn_{0.13}O_{1.4}$	2222	NR	NR	NR (*aRT, s*)	Minami[72] 1999
$Zn_{0.11}In_{0.80}Sn_{0.09}O_{1.5}$	4000	27	7	amorphous (*aRT, s*)	Minami et al.[74] 2000
$Zn_{0.12}In_{0.79}Sn_{0.09}O_{1.5}$	4350	20	5	amorphous (*a150, cs*)	Moriga et al.[75] 2000
$Zn_{0.23}In_{0.44}Sn_{0.33}O_{1.5}$	2290	NR	NR	In_2O_3 (*a450, m*)	Cui et al.[70] 2001
$Zn_{0.05}In_{0.86}Sn_{0.09}O_{1.5}$	2778	NR	NR	In_2O_3 (*A250, s*)	Chae[77] 2001
$Zn_{0.5}In_{0.48}Sn_{0.02}O_{1.2}$	2500	30	5	$Zn_2In_2O_5$ (*a500, p*)	Naghavi et al.[73] 2002
$Zn_{0.11}In_{0.86}Sn_{0.03}O_{1.5}$	2083	NR	NR	amorphous (*aRT, s*)	Sohn et al.[80] 2004
$Zn_{0.22}In_{0.44}Sn_{0.33}O_{1.5}$	2890	40	4.6	In_2O_3 (*A500, m*)	Ni et al.[68] 2005
$Zn_{0.2}In_{0.72}Sn_{0.08}O_{1.4}$	3333	9.5	11.8	amorphous (*aRT,cs*)	Liu et al.[84] 2006
$Zn_{0.2}In_{0.72}Sn_{0.08}O_{1.4}$	8333	347	1.6	In_2O_3 (*A325, cs*)	Mohamed[78] 2007
$Zn_{0.16}In_{0.70}Sn_{0.14}O_{1.5}$	2516	40	3.9	In_2O_3 (*aNR, p*)	Zhang et al.[79] 2007
$Zn_{0.34}In_{0.59}Sn_{0.07}O_{1.3}$	1526	18	5.3	amorphous (*aRT, cs*)	Liu et al.[83] 2008
$Zn_{0.11}In_{0.75}Sn_{0.14}O_{1.5}$	4000	NR	NR	In_2O_3 (*A400, p*)	Harvey et al.[45] 2008
$Zn_{0.05}In_{0.90}Sn_{0.05}O_{1.5}$	2631	NR	NR	amorphous (*aRT, s*)	Bae et al.[81] 2008
$Zn_{0.25}In_{0.50}Sn_{0.25}O_{1.5}$	1316	32	1.9	amorphous (*a300, s*)	Ow-Yang et al.[82] 2008

[a] The fifth column lists the reported phase and the deposition conditions in parentheses. Abbreviations - NR: not reported, *a*: as-deposited, *A*: annealed, *p*: PLD, *m*: MOCVD, *s*: sputtered, *cs*: co-sputtered, *RT*: room temperature, Numbers are temperatures in °C. Example: (*a450, s*) means as-deposited at 450 °C by sputtering. The formula stoichiometries are rewritten so that [Zn] + [In] + [Sn] = 1.0 to make comparing the relative percentage of each cation easier.

Table 2. Conductivities of Selected ITO Films[a]

nominal composition	σ (S·cm^{-1})	μ (cm^2 V^{-1} s^{-1})	n (×10^{20} cm^{-3})	phases (deposition)	reference
$In_{1.64}Sn_{0.36}O_3$	14,000	20−30	10	In_2O_3 (*a370, are*)	Nath et al.[6] 1980
$In_{1.82}Sn_{0.18}O_3$	7,700	35	15	In_2O_3 (*A500, sp*)	Frank and Kostlin[5] 1982
$In_{1.9}Sn_{0.1}O_3$	22,000	103	13.8	NR (*a300, ere*)	Rauf[7] 1993

[a] The fifth column lists the reported phase and the deposition conditions in parentheses. Abbreviations - *a*: as-deposited, *A*: annealed, *are*: activated reactive evaporation, *ere*: e-beam reactive evaporation, *sp*: spray pyrolysis. Numbers are temperatures in °C.

phase diagram was constructed at 1275 °C while $In_4Sn_3O_{12}$ does not form until 1345 °C.[64,65] $In_4Sn_3O_{12}$, however, has been grown as a thin film and conductivities greater than 1000 S/cm have been reported.[66,67] Although this phase will not be discussed with respect to ZITO films, it is another alternative for low-indium TCOs.

The cosubstitution of ZnO and SnO_2 into In_2O_3 demonstrated high conductivities in the bulk form, which initiated a number of thin-film studies.[45,68−71] ZITO films have also been explored as Sn-doped $(ZnO)_kIn_2O_{k+3}$ films[72,73] as well as codeposited ITO and ZnO.[74−76] Table 1 lists the highest conducting ZITO film reported from each study up through 2008. Table 2 lists several reported ITO films for comparison. It should be noted that the compositions and conductivity values are approximate.

Thin Film ZITO. All of the reported ZITO thin films have been plotted by composition in Figure 3. Two major observations can be made from this diagram. First, the conductivity has a mild sensitivity to the composition. There are no noticeable boundaries that would define an optimal composition. These results are promising from a manufacturing point of view because less indium is needed in ZITO than in ITO and less control of the composition is required to get conductive films. The second major observation, however, is the presence of a general trend where the conductivity increases with the percent indium. While many films have conductivities over 1000 S/cm, the most conductive films were observed in the In_2O_3-rich corner of the composition diagram. The percent transmission of the films are not explicitly mentioned or

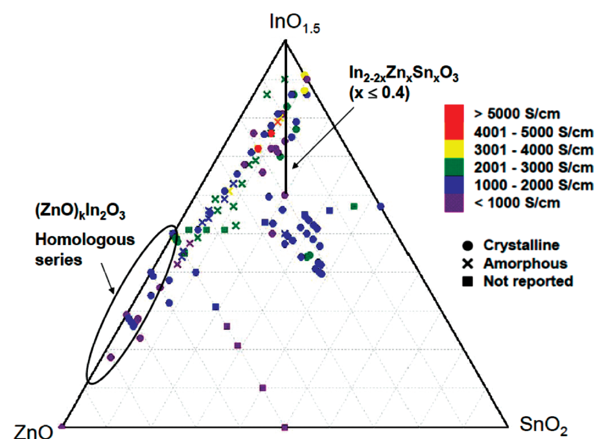

Figure 3. Reported ZITO films plotted by composition. Film denoted by a circle indicates the presence of at least one crystalline phase. Secondary amorphous phases may also have been present. Films marked with an "×" did not show a crystalline phase. Points marked with a square indicate the structure was not reported. The conductivities scale according to the color. Red, 5001+; orange, 4001−5000; yellow, 3001−4000; green, 2001−3000; blue, 1000−2000; purple, under 1000 S/cm.

discussed because all the films exhibited over 80% transmission for the visible range. The work function and etching rate can be tuned by adjustment of the composition (discussed later). The majority of reported thin film ZITO studies can be classified into three compositional areas: the $In_{2-2x}Sn_xZn_xO_3$ solid solution, the layered $(ZnO)_k(In_2O_3)$:Sn series and $(ITO)_{1-x}(ZnO)_x$ tie-line. Close examination of these results will show how the bulk equilibrium phases influence the properties of the thin films.

The $In_{2-2x}Sn_xZn_xO_3$ solid solution regime is where the highest conducting films have been observed. The films crystallized as the In_2O_3 structure[45,68,70,77−79] or were reported as amorphous.[80−82] The equilibrium cosubstitution is [Sn] = [Zn], but as seen in Figure 3, many of the film compositions deviated from this line. The films were n-type regardless if [Sn]/[Zn] > 1 (excess Sn donors) or if [Sn]/[Zn] < 1 (excess Zn acceptors), which is the same behavior that was observed for the bulk. Harvey et al.[45] grew a series of crystalline ZITO films near the $In_{2-2x}Zn_xSn_xO_3$ solid solution with different [Sn]/[Zn] ratios. They observed as-deposited conductivities that ranged from 100−3700 S/cm depending on the composition. The film composition was controlled by the partial oxygen pressure (pO_2) during the deposition. As the pO_2 increased, the [Sn]/[Zn] ratio decreased. The film compositions, which resulted from each deposition, are shown in Figure 4 with the conductivity and optical absorption dependence as a function of pO_2. A spike in conductivity and dip in the absorption coefficient occurred when the [Sn]/[Zn] ratio was slightly higher than one, which corresponded to Sn-excess $In_{2-2x}Zn_xSn_xO_3$.[45] This composition is also where the bulk $In_{2-2x}Sn_xZn_xO_3$ solid solution exhibited the highest conductivities.[45] Reduction treatments of ZITO films near the $In_{2-2x}Zn_xSn_xO_3$ solid solution improved the conductivity, but ZITO films exhibited lower sensitivity to reduction treatments than ITO.[45,68] Harvey et al.[45] showed that the dominant defect in bulk $In_{2-2x}Sn_xZn_xO_3$ may be an inherent off-stoichiometry of Sn and Zn such that [Sn] > [Zn], which generates conduction electrons. The conductivity dependence of $In_{2-2x}Zn_xSn_xO_3$ on the pO_2 may then be explained by these Sn donors forming Frank−Köstlin associates.[45]

Thin films of Sn-doped $(ZnO)_kIn_2O_3$ have been explored as low-indium TCOs.[42,73] The different $(ZnO)_k$-In_2O_3:Sn studies showed the same trends—the conductivity decreased as the percentage of indium decreased and the conductivity was improved when doped with less than 5% Sn.[42,73] The films exhibited the same behavior as bulk $(ZnO)_kIn_2O_3$ where the conductivity declined as the percent indium was lowered[51,62] and low levels of Sn doping improved the conductivity.[62,63] While Sn-doping raised the conductivity of $(ZnO)_kIn_2O_3$, the improvement was typically less than a factor of 2 for both bulk and thin films.[42,62,63,73] Reducing treatments of $(ZnO)_k(In_2O_3)$:Sn films showed mild sensitivity to pO_2 compared to ITO films. Liu et al.[83] used a reducing anneal to improve a $(ZnO)_k(In_2O_3)$:Sn film by less than 50% whereas reduction of an ITO film, prepared with the same deposition conditions, improved the conductivity by 1000%. This conductivity behavior suggests that Sn donors are not the primary defect by which carriers are generated in the structure.[83] The bulk $(ZnO)_kIn_2O_3$ phases exhibit the same minor conductivity improvement upon reducing treatments.[51] The $(ZnO)_kIn_2O_3$ defect chemistry is poorly understood, and a better understanding of these bulk phases would help elucidate the electrical behavior of the thin films.

The $(ITO)_{1-x}(ZnO)_x$ tie-line is a popular regime to explore because series of these films can be grown by

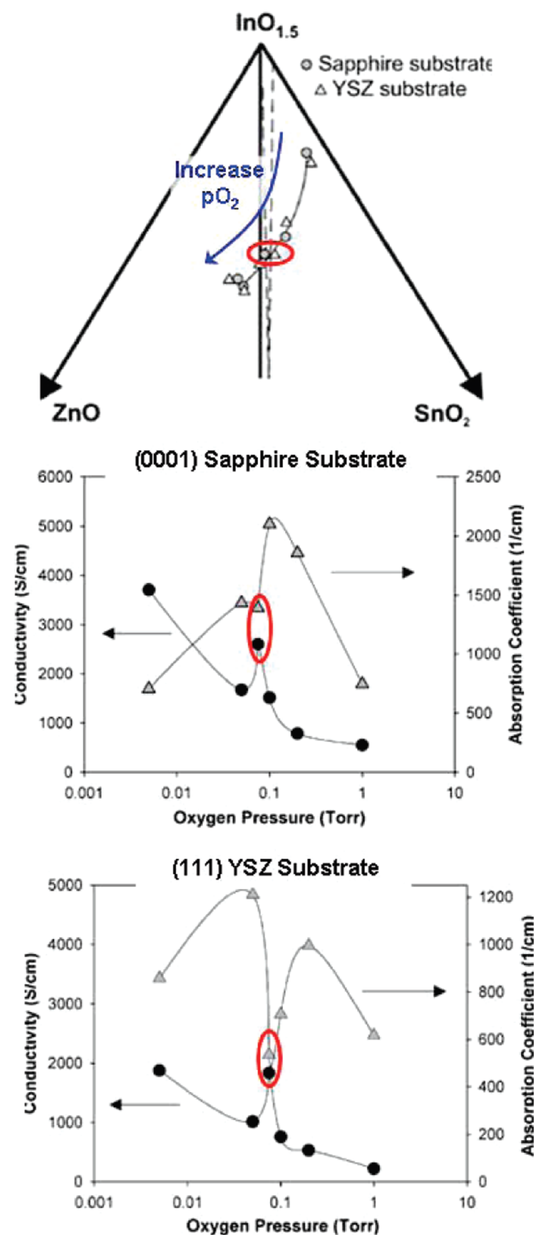

Figure 4. ZITO films prepared by PLD on c-plane sapphire and YSZ-(111) at a series of partial oxygen pressures. Image on top shows the films plotted by composition, and the arrow denotes the increase of pO_2 for each deposition. Bottom two images show the conductivity from each as-deposited film as a function of pO_2 during deposition. Curved arrow denotes the change of composition with the decreasing [Sn]/[Zn] ratio. The compositions of the circled points on the top image corresponds to the conductivity of the circled points on the bottom images. Reprinted and modified (circles and arrow on top image were drawn in) with permission from Harvey et al.[44]. Copyright 2008 Wiley-Blackwell.

codeposition of ITO and ZnO targets.[74,75,78,84,85] The $(ITO)_{1-x}(ZnO)_x$ tie-line can be split into three separate sections: the ITO-rich end, the middle and the ZnO-rich end. The film conductivities are plotted in Figure 5 as a function of x along the $(ITO)_{1-x}(ZnO)_x$ tie-line. The ITO-rich films ($x < 0.2$) had nominal compositions near the $In_{2-2x}Zn_xSn_xO_3$ solid solution line and are where the highest conducting films were observed. Many of the film compositions were observed on the Zn-excess side of the solid solution line because the Sn concentration had an upper limit of 10%. The ITO-rich films exhibited the

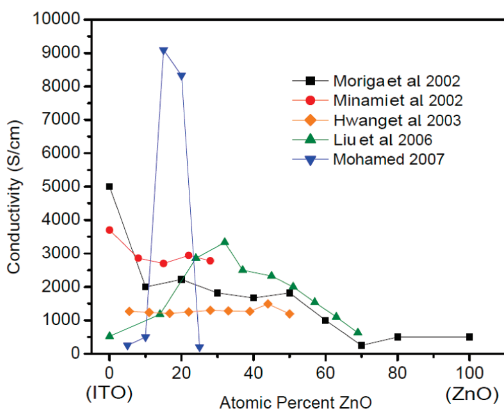

Figure 5. Conductivity of codeposited $(ITO)_{1-x}(ZnO)_x$ films. Notice the non-linear dependence of the conductivity as a function of the nominal composition between the end points. Data redrawn from references 74,75,78,84,85.

same behavior as the $In_{2-2x}Sn_xZn_xO_3$ films and, hence, bulk $In_{2-2x}Sn_xZn_xO_3$. They had the high n-type conductivities and crystallized to bixbyite In_2O_3.[74,75,78,85,86] It was in this regime that the highest ZITO conductivities were reported by Mohamed.[78] ZnO was not observed as a secondary phase at the ITO-rich regime with one possible exception,[78] which supports the formation of the cosubstituted $In_{2-2x}Zn_xSn_xO_3$ phase as opposed to a physical mixture of ITO and ZnO.[74,75,78,85,86]

Films in the middle of the $(ITO)_{1-x}(ZnO)_x$ tie-line ($x \approx 0.2-0.55$) were consistently amorphous.[74,75,78,86] Liu et al.[83] annealed amorphous $(ITO)_{0.66}(ZnO)_{0.34}$ at 700 °C, which crystallized to a mixture of In_2O_3 and $Zn_2In_2O_5$. $Zn_2In_2O_5$ was not present in the subsolidus phase diagram (Figure 1) because it does not form until 1550 °C,[52] but it has been grown as a thin film.[87,88] Liu et al.[83] annealed amorphous $(ITO)_{0.4}(ZnO)_{0.6}$ at 700 °C to form a mixture of In_2O_3 and $Zn_3In_2O_6$. According to the subsolidus phase diagram, the equilibrium phases for the given composition are In_2O_3, $Zn_3In_2O_6$, and Zn_2SnO_4.[12] The crystalline phases in the film agree with the expected bulk phases except for the absence of Zn_2SnO_4 in the film. The Zn_2SnO_4 may have gone undetected, though, as broad peaks in the XRD pattern. Another possibility is that Sn could have doped In_2O_3 or $Zn_3In_2O_6$ in the film rather than precipitate out as Zn_2SnO_4. It is possible for the cations to be segregated and for nanosized ordered regions and crystallites to form. Hwang et al.[85] observed bixbyite In_2O_3 for $(ITO)_{1-x}(ZnO)_x$ for $x = 0-0.45$. An amorphous film was not seen until $x = 0.5$. The crystallinity for $x = 0.2-0.45$ does not seem consistent with the other $(ITO)_{1-x}(ZnO)_x$ reports mentioned above. Hwang et al.[85] analyzed the composition of the amorphous $(ITO)_{0.5}(ZnO)_{0.5}$ film as a function of film depth and observed a depletion of Zn in the middle of the film with an excess of Zn near the substrate. The amorphous $(ITO)_{0.5}(ZnO)_{0.5}$ film was actually ITO atop a ZnO buffer layer rather than a homogeneous $In_{0.45}Sn_{0.05}Zn_{0.5}O_x$ type film.[85] Although the composition depth profile of the crystalline films were not analyzed, it is reasonable to expect that they would exhibit the same microstructure owing to the similar deposition conditions. Therefore, the crystallinity of the $(ITO)_{1-x}(ZnO)_x$ films grown by Hwang et al.[85] was likely due to the formation of separate ITO and ZnO layers.

ZnO-rich films ($x > 0.55$) crystallized as $(ZnO)_kIn_2O_3$ and ZnO.[75,86] ZnO was not observed until the end of the $(ITO)_{1-x}(ZnO)_x$ tie-line ($x > 0.7$).[75,86] The reports did not mention a shift of the ZnO XRD peaks to indicate In doping. The crystalline k-phases, which were seen in the films, corresponded to the equilibrium phases for the same compositions. Liu et al.[86] observed $(ZnO)_kIn_2O_3$ but was not able to determine which k-phases were present. Moriga et al.[75] observed the phase $Zn_3In_2O_6$ for a $(ITO)_{0.43}$-$(ZnO)_{0.57}$ film and $Zn_5In_2O_8$ for a $(ITO)_{0.34}(ZnO)_{0.66}$ film. At equilibrium the nominal composition $(ITO)_{0.43}(ZnO)_{0.57}$ will form $Zn_3In_2O_6$, In_2O_3, and Zn_2SnO_4. The composition $(ITO)_{0.34}(ZnO)_{0.66}$ will form $Zn_5In_2O_8$, $Zn_4In_2O_7$, and Zn_2SnO_4. Films at the ZnO-rich end of the $(ITO)_{1-x}(ZnO)_x$ tie-line had lower conductivities than films deposited at the ITO-rich end.[75,86] This conductivity trend is the same for bulk equilibria—the $In_{2-2x}Sn_xZn_xO_3$ solid solution is more conductive than $(ZnO)_k(In_2O_3)$:Sn, and the conductivity of each k-phase decreases with increasing k (less In).[45,51,62]

Characterization. Structural characterization of the films is necessary to understand the electrical and optical properties. Although many of the crystalline films denoted in Figure 3 are reported to be single-phase, most of them do not appear on single-phase lines. Film microstructures were determined most commonly by XRD. Crystalline phases are apparent, but nanosized crystallites or amorphous regimes may go undetected. Films that are oriented will only diffract the favored lattice planes. As a result the XRD patterns of thin films may only show a few peaks, which makes the phase identification less certain. If the film is on a crystalline substrate, glancing angle X-ray diffraction may be necessary to avoid saturation of the detector by the substrate peaks. Synchrotron facilities offer high flux beams and are equipped with area plate detectors for transmission XRD. Synchrotrons also offer the ability to do microdiffraction and X-ray absorption spectroscopy. Other techniques such as electron microscopy and electron diffraction can be used to examine the film quality and probe the homogeneity of the microstructure.

ZITO films have been deposited both in the crystalline and amorphous state. The degree of crystallinity can be controlled with the substrate temperature, substrate crystallinity, post-deposition annealing temperature, and composition. Films deposited at room temperature on glass tend to be amorphous,[42,81,86] whereas films deposited on sapphire heated to 500 °C will be crystalline.[45,79,89] Undoped In_2O_3 films easily crystallize; addition of the smaller Zn and Sn cations stabilize amorphous films and increase the temperature of crystallization.[81,83] Amorphous films pose an extra challenge for characterization. As a result, the homogeneity and local structure of amorphous films are poorly understood. "Amorphous" films are assumed to be glass-like with a uniform composition, but this assumption has not been verified. It is

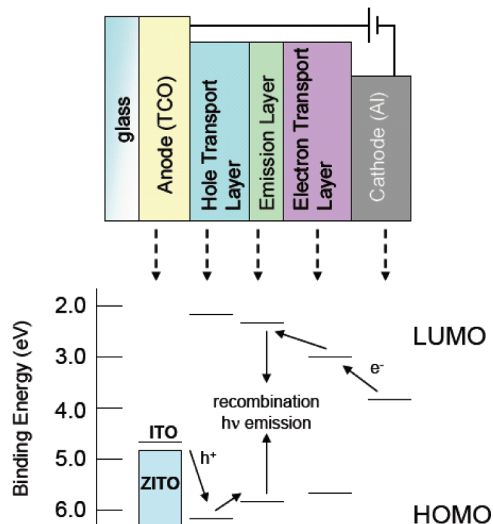

Figure 6. Cartoon of OLED schematic. The relative energy levels are plotted below the corresponding component. The approximate location of LUMO/HOMO energy levels are redrawn from Cui et al.[69].

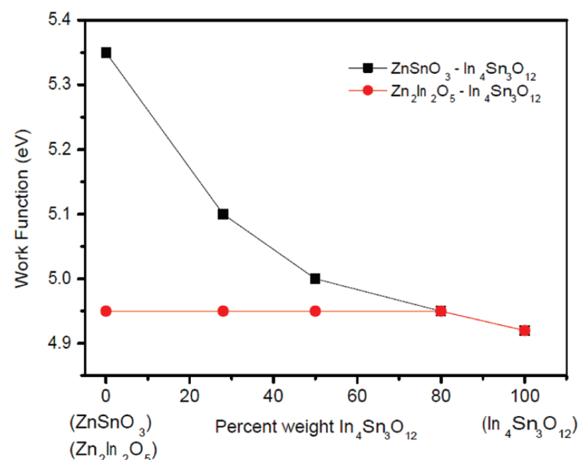

Figure 7. Work function of films with composition $(100 - x)ZnSnO_3 - (x)In_4Sn_3O_{12}$ (squares) and $(100 - x)Zn_2In_2O_5 - (x)In_4Sn_3O_{12}$ (circles) by percent weight. Data are from Minami.[71] The resistivity corresponding to each composition was not reported.

possible for the cations to be segregated and for nanosized crystallites and phases to exist. The structure type affects how the material generates and conducts electrons, so it is critical to investigate and understand these oxides that do not exhibit long-range order.

The relative ratios between the cations in the films are difficult to control with deposition techniques, especially for ternary systems and multiple-target depositions. The composition is commonly determined by energy dispersive spectrometry (EDS) that is commonly attached to scanning electron microscopes (SEM). The elemental composition of the sample probed by the electron beam can then be determined by standard-less analysis, but external standards should be used to obtain a composition within a 10% uncertainty.[90] A single EDS measurement will not necessarily reflect the average film composition because it will be limited to the sampling volume probed by the beam. This site-specific measurement, however, can be used to assess the homogeneity of the film composition. Hwang et al.[85] measured the composition of an amorphous $(ITO)_{0.5}(ZnO)_{0.5}$ cosputtered film and observed a significant Zn gradient that was concentrated near the substrate. Homogeneity of the Zn:In:Sn ratios should be examined, especially for codepositions and amorphous films, because the composition will influence the phase formation.

Work Function and Etching Rate. If TCOs are to be applicable they must satisfy the electronic requirements of the device. The work function of an LED should match the highest occupied molecular orbital (HOMO) of the hole-transport layer to achieve maximum efficiency of hole transport to the emission layer. A schematic of an organic LED (OLED) over the relative HOMO and lowest unoccupied molecular orbital (LUMO) energy levels is shown in Figure 6. ITO has a work function around 4.7 eV,[91] which is not necessarily aligned with the HOMO of the hole transport layer. The reported work function of ZITO changes as a function of composition ranging from 4.9 to 6.1 eV, the latter being for the composition $Zn_2In_3Sn_4O_{14}$ ($2ZnO-In_3Sn_4O_{12}$).[70,72] Figure 7 plots the work functions of two series of ZITO films as a function of composition. The films composed along the $ZnSnO_3-In_4Sn_3O_{12}$ tie-line had work functions that ranged from 4.9 to 5.35 eV whereas films composed along the $Zn_2In_2O_5-In_4Sn_3O_{12}$ tie-line had a constant work function at 4.95 eV. It should be noted that the compositions are nominal, and the phases for each film were not reported. Cui et al.[70] fabricated two OLEDs, one with an ITO anode and another with a $Zn_{0.45}In_{0.88}Sn_{0.66}O_{3-\delta}$ anode. The HOMO of the hole injection layer was 6.0 eV and was aligned closer to ZITO at 6.1 eV than ITO at 4.7 eV. The OLED with the ZITO anode generated more than twice the maximum forward light output than the OLED with ITO. The tunable work function of ZITO is advantageous for device integration because it can be tailored to a specific interfaced layer.[68,70,81]

The etching rate is an important, yet overlooked, property in TCOs. Some device applications prefer a fast etching rate to quickly clean the surface. Other device applications, however, use corrosive active-layers, so the TCO must be robust to prevent early degradation. Minami[72] showed how a series of ZITO films were tuned to have a fast etching rate or minimal etching by adjustment of the composition (Figure 8). The conductivity of these films stayed within the range 140−750 S/cm. Ni et al.[68] tested two OLEDs, one with a $ZnIn_2Sn_{1.5}O_x$ anode and the other with an ITO anode. The anodes were spin-cast with a common hole-injection layer known as PEDOT-PSS, poly(3,4-ethylenedioxythiophene) poly(styrenesulfonate). Approximately 1% of the ITO anode was dissolved by the PEDOT-PSS, but less than 0.05% of the ZITO anode was dissolved by the PEDOT-PSS. The ZITO-based OLED had a higher light output than the ITO-based OLED, which was attributed to the chemical robustness of ZITO over ITO.[68] Although ZITO may be less conductive than ITO, the tunability of the work function and etching rate makes ZITO a strong contender against ITO for device optimization and sustainability.

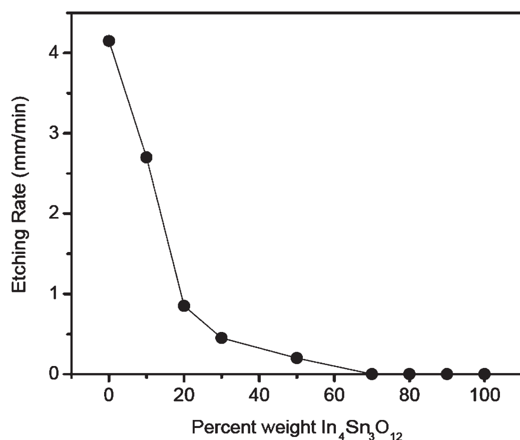

Figure 8. Etching rate of films with composition $(100 - x)Zn_2In_2O_5 - (x)In_4Sn_3O_{12}$ by percent weight. Data replotted from Minami.[71]

ZITO as a Transparent Semiconductor. There is now interest in the development of devices where every component is transparent.[92−94] Electrically active transparent oxides can be utilized in a new manner, specifically, as amorphous transparent oxide semiconductors (*a*-TOS). An *a*-TOS would be used as a channel layer for thin film transistors (TFT), replacing the currently used amorphous hydrogenated silicon (*a*-Si:H). Replacing the remaining components of the transistor with transparent materials will lead to fully transparent electronics. The benefits and development of transparent electronics and their technological implications has been reviewed thoroughly.[95]

The distinguishing difference between a TCO and an *a*-TOS is the carrier density. A TCO should have carrier densities on the order of 10^{21} cm^{-3} to exhibit high conductivities for improved device efficiency. An *a*-TOS carrier density is limited to 10^{17} cm^{-3} to prevent charge leakage and enable high on-to-off ratios in TFTs. With such low carrier densities the tunneling current drops and grain boundaries become a significant source of electron traps. It has been suggested that growing films in an amorphous state eliminates grain boundaries. The crystalline structure of a TOS is known, but the local structure of an amorphous TOS and its relationship to the crystalline structure has not been extensively investigated.[96] It has been shown by experiment[97−99] and theory[100] that the carrier mobilities are the same between the amorphous and crystalline states of an *a*-TOS, which is not the case for the semiconductor Si.[101] The spherical geometry of the *ns* conduction orbitals in the *a*-TOS overlap regardless of the bond orientation, so electrons have the same mobility for the crystalline and amorphous state. The sp^3 orbitals in Si, on the other hand, are highly directed and lose significant overlap when the crystal structure loses order. As a result, the mobilities of an *a*-TOS (10−20 $cm^2/(V\ s)$) are higher than *a*-Si:H (∼1 $cm^2/(V\ s)$). Because the target electronic properties for an *a*-TOS differ from a TCO, new compositions and structures need to be explored.

Grover et al.[102] made a TFT with the channel layer $In_{0.20}Sn_{0.75}Zn_{0.05}O_x$. The transistor was not fully transparent and had a large negative turn-on voltage, which indicated that the transistor operated in depletion mode. The ZITO channel did have, however, an effective mobility of 15 $cm^2/(V\ s)$ and an on-to-off ratio of 10^7. Buchholz et al.[103] fabricated a TFT with an $In_{1.4}Sn_{0.27}Zn_{0.33}O_{3-\delta}$ channel that had a field effect mobility $\mu = 10\ cm^2/(V\ s)$, on-to-off ratio of 10^6, and a positive threshold voltage indicating that the transistor operated in enhancement mode. The channel layer was tuned by the pO_2 deposition to be either a degenerate or nondegenerate semiconductor. The high pO_2 during film deposition trapped the free electrons and lowered the carrier concentration to an appropriate level for a TFT channel layer.[103] This same conduction behavior was mentioned previously in the bulk ZITO section where Ambrosini et al.[48] observed a transition from degenerate to nondegenerate conductivity for bulk $In_{2-2x}Sn_xZn_xO_3$ after subjecting the powder to oxidative annealing. Successful transparent TFTs with other *a*-TOS channel layers, such as Zn_2SnO_4 and $InGaZnO_4$ have been fabricated.[32,100,104] Transparent TFTs have also been fabricated with crystalline undoped In_2O_3 and ZnO channel layers,[32,92,93,104−106] which demonstrates that the amorphous structure is not necessarily required. If the channel layer contains large grains, then there will be few grain boundaries to trap the carriers. The field of *a*-TOSs and transparent transistors is still emerging and ZITO will play an integral role in the development of transparent electronics.

ZnO-SnO₂ or ZTO System. One goal of TCO research is to develop low-cost TCOs with conductivities and transparencies as high as ITO. An attractive system to study is $ZnO-SnO_2$ (ZTO). ZTO currently is used as a resistive component in a variety of applications, such as varistors,[107,108] gas sensors,[109−111] and CdTe solar cell buffer layers.[112] ZTO has recently been examined quite extensively as an inexpensive TCO.[113−128] ZTO has been the subject of numerous high-throughput combinatorial film growth studies.[113−119,128] Owing to the development of multitarget vapor deposition film growth techniques, a series of films that vary in composition can be grown during a single deposition. These combinatorial film growth techniques can also investigate how a series of films is affected by substrate temperature, atmosphere, or post-deposition annealing.

One prominent feature of the combinatorial studies was the non-linear conductivity dependence on composition. The relative percentage of Zn and Sn affected the electrical properties, but there was not a well-defined relationship between the conductivity of the unary oxide end-members and the binary films. Furthermore, not every film study observed the same conductivity versus composition trend. Minami et al.[113−115] and Moriga et al.[117] observed a spike in conductivity at [Zn]:[Sn] = 40:60. This Zn:Sn ratio does not correspond with a known zinc tin oxide phase. Conversely, Perkins et al.[118,119] observed spikes in the conductivity for [Zn]:[Sn] = 60:40 and [Zn]:[Sn] = 50:50. These compositions correspond to the known Zn_2SnO_4 spinel and the metastable $ZnSnO_3$. Bulk powder conductivity measurements of Zn_2SnO_4 reveal a high resistivity.[43] $ZnSnO_3$ is metastable with two reported polymorphs: ilmenite[129] and $LiNbO_3$-type.[130] Both polymorphs have been synthesized as a bulk powder, but the

Table 3. Conductivities of Top-Performing ZTO Films[a]

nominal composition	σ (S·cm^{-1})	μ (cm^2 V^{-1} s^{-1})	n (× 10^{20} cm^{-3})	phases (deposition)	reference
$Sn_{0.73}Zn_{0.27}O_{1.8}$	250	15	1	amorphous (*aRT, s*)	Minami et al.[114] 1994
$Sn_{0.5}Zn_{0.5}O_{1.5}$	240	30	0.5	NR (*A400, p*)	Perkins et al.[118] 2002
$Sn_{0.98}Zn_{0.02}O_2$	200	4	8	SnO_2 (*a250, cs*)	Moriga et al.[117], Hayashi et al.[116] 2004
$Sn_{0.6}Zn_{0.4}O_{1.2}$	250	18	0.8	amorphous (*a300, v*)	Minami et al.[115] 2005
$Sn_{0.92}Zn_{0.08}O_{1.9}$	1000	25	2	SnO_2 (*A300, cs*)	Ko et al.[132] 2006
$Sn_{0.89}Zn_{0.11}O_{1.9}$	526	25	1.5	amorphous (*A450, cs*)	Ko et al.[128] 2007

[a] The fifth column lists the reported phase and the deposition conditions in parentheses. Abbreviations − NR: not reported, *a*: as-deposited, *A*: annealed, *v*: vacuum arc plasma evaporation, *s*: sputtering, *cs*: co-sputtering, *p*: pulsed laser deposition. Numbers are temperatures in °C.

conductivity was not measured because sintering a dense pellet requires temperatures beyond the stability threshold of $ZnSnO_3$. An epitaxial film of $ZnSnO_3$ was grown, but the conductivity was not measured.[131] ZTO films tend to be amorphous when there is more than 20% of each metal present.[114−117,128] When the amorphous films are annealed to the point of crystallization, mixtures of ZnO, SnO_2, and Zn_2SnO_4 are seen.[116,128] The intermediary binary phases influence the electrical properties of ZTO films, as seen by the fluctuations of ZTO films as a function of composition.[113−119] But, the trends observed from the various reports[113−115,117−119] are not consistent with one another, so the influence of the bulk phases is unclear. To improve ZTO films to compete with ITO and ZITO, the conduction behavior must be better understood.

Of all the film studies, the highest reported conductivity of a ZTO film has been 1,000 S/cm.[132] The conductivities of ZTO films are an order of magnitude less than ITO and ZITO. The highest reported ZTO films are listed in Table 3. It can be seen that both the mobilities and carrier concentrations of ZTO films are lower than those listed for ITO and ZITO. An understanding of the defect chemistry can offer insight as to effective dopants, which can improve the electron concentration and make ZTO a competitor to ITO. Although ZTO may not replace ITO in high-end electronics, ZTO can be a low-cost TCO layer for applications that do not require high conductivities.

ZTO has also been examined as an *a*-TOS and implemented into transistors.[133−138] ZTO has shown excellent performance as a channel layer for transparent TFTs owing to its tendency to be amorphous with high optical transparency and high electron mobilities. Chiang et al.[133] fabricated transparent TFTs using an amorphous ZTO channel layer and observed a field effect mobility $\mu = 25$ cm^2/(V s), on-to-off ratio of 10^7 and a positive threshold voltage. ZTO films have been fabricated using the physical vapor deposition techniques mentioned earlier and solution processing techniques such as sol−gel spin-coating.[134,135,137] ZTO will likely become a popular channel layer for TFTs owing to its low cost, ease of thin film fabrication, and promising device performance.

Conclusion

ZITO (Zn-In-Sn-O) materials are promising replacements for ITO as the TCO layer in many opto-electronic applications. ZITO contains less indium than ITO, which lowers the cost, and it has a broad window of compositions that allow the TCO layer to be tuned (conductivity, work function, etc.) for each application. The bulk equilibrium phases of ZITO have been well-defined and exhibit two transparent and conductive regions: the $In_{2-2x}Zn_xSn_xO_3$ solid solution and the $(ZnO)_kIn_2O_3$ homologous series. ZITO thin films, however, have been grown across a vast array of compositions by a variety of deposition methods. Nevertheless, the thin films can be classified into the same two categories: the $In_{2-2x}Zn_xSn_xO_3$ solid solution and $(ZnO)_kIn_2O_3$:Sn homologous series. The thin film studies defined a third regime: the $(ITO)_{1-x}(ZnO)_x$ binary. It was shown that the films grown along this binary can also be described by the $In_{2-2x}Zn_xSn_xO_3$ and $(ZnO)_kIn_2O_3$:Sn regimes. Although select films were deposited in states of non-equilibrium, the films exhibited conduction behavior that was similar to the bulk phases. Knowledge of the carrier generation mechanisms in the bulk phases is important for understanding the electrical behavior of these thin films. The bulk phase diagram can be a guide for identifying highly conductive regimes, and the thin film diagram reveals which regions have already been explored. As an example, few thin films have been grown on the Sn-excess side of the $In_{2-2x}Zn_xSn_xO_3$ solid solution, but the bulk equilibrium behavior predicts modest conductivities. Current knowledge of the electrical behavior of ZITO has led to a controlled lowering of the carrier content to semiconducting levels for utilization as amorphous oxide semiconductors (*a*-TOS). The application of ZITO in electronic devices can then expand to transistors and transparent electronics. A likely candidate material for a TCO is ZTO (Zn-Sn-O), owing to its inexpensive raw materials and ease of manufacturing. Although ZTO has not been able to replicate the high conductivities demonstrated by ITO and ZITO, further research on the carrier generation mechanisms and electrical behavior is warranted. ZTO is a suitable alternative for applications that do not demand high conductivities. ZTO has also shown to be an effective *a*-TOS and is being developed for transparent electronics (e.g., transparent transistor applications).

Acknowledgment. C.A.H. was funded by the Materials Research Science and Engineering Center at Northwestern University supported by the National Science Foundation under NSF Award Number DMR-0520513. The authors gratefully acknowledge additional support from the Department of Energy Basic Energy Sciences (Award No. DE-FG02-08ER46536, crystalline ZITO work) and the Energy Frontier Research Center at the ANSER Center of Northwestern University under contract No. DE-SC0001059 (amorphous ZITO work).

References

(1) Fortunato, E.; Ginley, D.; Hosono, H.; Paine, D. C. *MRS Bull.* **2007**, *32*, 242.
(2) Porch, A.; Morgan, D. V.; Perks, R. M.; Jones, M. O.; Edwards, P. P. *J. Appl. Phys.* **2004**, *95*, 4734.
(3) Marks, T. J.; Veinot, J. G. C.; Cui, J.; Yan, H.; Wang, A.; Edleman, N. L.; Ni, J.; Huang, Q.; Lee, P.; Armstrong, N. R. *Synth. Met.* **2002**, *127*, 29.
(4) Ginley, D. S.; Bright, C. *MRS Bull.* **2000**, *25*, 15.
(5) Frank, G.; Kostlin, H. *Appl. Phys. A: Mater. Sci. Process.* **1982**, *27*, 197.
(6) Nath, P.; Bunshah, R. F.; Basol, B. M.; Staffsud, O. M. *Thin Solid Films* **1980**, *72*, 463.
(7) Rauf, I. A. *Mater. Lett.* **1993**, *18*, 123.
(8) Carlin, J. F., Jr. In *United States Geological Survey: Mineral Commodity Summary*; minerals.usgs.gov/minerals/pubs/commodity/indium/indiumcs06.pdf, 2007; pp 78−79.
(9) Brown, R. D., Jr. In *United States Geological Survey: Minerals Commodity Summary*; minerals.er.usgs.gov/minerals/pubs/commodity/indium/490798.pdf, 1999; pp 57−59.
(10) Tolcin, A. C. In *United States Geological Survey: Mineral Commodity Summary*; minerals.usgs.gov/minerals/pubs/commodity/indium/mcs-2009-indiu.pdf, 2009; pp 76−77.
(11) Palmer, G. B. Doctoral Thesis for the Department of Chemistry, Northwestern University, 1999.
(12) Harvey, S. P.; Poeppelmeier, K. R.; Mason, T. O. *J. Am. Ceram. Soc.* **2008**, *91*, 3683.
(13) Hamberg, I.; Granqvist, C. G. *J. Appl. Phys.* **1986**, *60*, R123.
(14) Edwards, P. P.; Porch, A.; Jones, M. O.; Morgan, D. V.; Perks, R. M. *Dalton Trans.* **2004**, 2995.
(15) Mryasov, O. N.; Freeman, A. J. *Phys. Rev. B.* **2001**, *64*, 233111.
(16) Bertoni, M. I.; Mason, T. O.; Medvedeva, J. E.; Freeman, A. J.; Poeppelmeier, K. R.; Delley, B. *J. Appl. Phys.* **2005**, *97*, 103713.
(17) Meng, Y.; Yang, X.; Chen, H.; Shen, J.; Jiang, Y.; Zhang, Z.; Hua, Z. *Thin Solid Films* **2001**, *394*, 219.
(18) Meng, Y.; Yang, X.; Chen, H.; Shen, J.; Jiang, Y.; Zhang, Z.; Hua, Z. *J. Vac. Sci. Technol. A* **2002**, *20*, 288.
(19) Medvedeva, J. E. *Europhys. Lett.* **2007**, *78*, 57004.
(20) Kawazoe, H.; Ueda, K. *J. Am. Ceram. Soc.* **1999**, *82*, 3330.
(21) Abrahams, S. C.; Bernstein, J. L. *Acta Crystallogr., Sect. B* **1969**, *25*, 1233.
(22) Parthé, E. *Crystal Chemistry of Tetrahedral Structures*, Gordon and Breach Science Publishers: New York, 1964.
(23) Marezio, M. *Acta Crystallogr.* **1966**, *20*, 723.
(24) Wyckoff, R. W. G. *Crystal Structures*; Interscience Publishers: New York, 1958; Vol. *1*.
(25) Frank, G.; Brock, L.; Bausen, H. D. *J. Cryst. Growth* **1976**, *36*, 179.
(26) Frank, G.; Kostlin, H.; Rabenau, A. *Phys. Status Solidi A* **1979**, *52*, 231.
(27) Gonzalez, G. B.; Mason, T. O.; Quintana, J. P.; Warschkow, O.; Ellis, D. E.; Hwang, J.-H.; Hodges, J. P.; Jorgensen, J. D. *J. Appl. Phys.* **2004**, *96*, 3912.
(28) Parent, P.; Dexpert, H.; Tourillon, G.; Grimal, J.-M. *J. Electrochem. Soc.* **1992**, *139*, 276.
(29) Parent, P.; Dexpert, H.; Tourillon, G.; Grimal, J.-M. *J. Electrochem. Soc.* **1992**, *139*, 282.
(30) Lany, S.; Zunger, A. *Phys. Rev. Lett.* **2007**, *98*, 45501.
(31) Tanaka, I.; Tatsumi, K.; Nakano, M.; Adachi, H.; Oba, F. *J. Am. Ceram. Soc.* **2002**, *85*, 68.
(32) Wang, L.; Yoon, M.-H.; Facchetti, A.; Marks, T. J. *Adv. Mater.* **2007**, *19*, 3252.
(33) Wang, C. Y.; Cimalla, V.; Romanus, H.; Kups, T.; Niebelschutz, M.; Ambacher, O. *Thin Solid Films* **2007**, *515*, 6611.
(34) De Wit, J. H. W.; van Unen, G.; Lahey, M. *J. Phys. Chem. Solids* **1977**, *38*, 819.
(35) Ali, E. B.; Maliki, H. E.; Bernede, J. C.; Sahnoun, M.; Khelil, A.; Saadane, O. *Mater. Chem. Phys.* **2002**, *73*, 78.
(36) Adurodija, F. O.; Semple, L.; Bruning, R. *J. Mater. Sci.* **2006**, *41*, 7096.
(37) Kaleemulla, S.; Reddy, A. S.; Uthanna, S.; Reddy, P. S. *J. Alloys Compd.* **2009**, *479*, 589.
(38) Yang, Y.; Huang, Q. L.; Metz, A. W.; Ni, J.; Jin, S.; Marks, T. J.; Madsen, M. E.; DiVenere, A.; Ho, S. T. *Adv. Mater.* **2004**, *16*, 321.
(39) Bellingham, J. R.; Phillips, W. A.; Adkins, C. J. *J. Phys.: Condens. Matter* **1990**, *2*, 6207.
(40) Gonzalez, G. B.; Cohen, J. B.; Hwang, J.-H.; Mason, T. O.; Hodges, J. P.; Jorgensen, J. D. *J. Appl. Phys.* **2001**, *89*, 2550.
(41) Warschkow, O.; Ellis, D. E.; Gonzalez, G. B.; Mason, T. O. *J. Am. Ceram. Soc.* **2003**, *86*, 1700.
(42) Phillips, J. M.; Cava, R. J.; Thomas, G. A.; Carter, S. A.; Kwo, J.; Siegrist, T.; Krajewski, J. J.; Marshall, J. H.; W. F. Peck, J.; Rapkine, D. H. *Appl. Phys. Lett.* **1995**, *67*, 2246.
(43) Palmer, G. B.; Poeppelmeier, K. R.; Mason, T. O. *J. Solid State Chem.* **1997**, *134*, 192.
(44) Palmer, G. B.; Poeppelmeier, K. R.; Mason, T. O. *Chem. Mater.* **1997**, *9*, 3121.
(45) Harvey, S. P.; Mason, T. O.; Buchholz, D. B.; Chang, R. P. H.; Korber, C.; Klein, A. *J. Am. Ceram. Soc.* **2008**, *91*, 467.
(46) Seo, K.-H.; Park, D.-H.; Lee, J.-H.; Kim, J.-J. *Solid State Ionics* **2006**, *177*, 601.
(47) Bizo, L.; Choisnet, J.; Retoux, R.; Raveau, B. *Solid State Commun.* **2005**, *136*, 163.
(48) Ambrosini, A.; Malo, S.; Poeppelmeier, K. R.; Lane, M. A.; Kannewurf, C. R.; Mason, T. O. *Chem. Mater.* **2002**, *14*, 58.
(49) Yanagi, H.; Hase, T.; Ibuki, S.; Ueda, K.; Hosono, H. *Appl. Phys. Lett.* **2001**, *78*, 1583.
(50) Mason, T. O.; Kammler, D. R.; Ingram, B. J.; Gonzalez, G. B.; Young, D. L.; Coutts, T. J. *Thin Solid Films* **2003**, *445*, 186.
(51) Moriga, T.; Edwards, D. D.; Mason, T. O.; Palmer, G. B. Poeppelmeier, K. R.; Schindler, J. L.; Kannewurf, C. R.; Nakabayashi, I. *J. Am. Ceram. Soc.* **1998**, *81*, 1310.
(52) Kasper, V. Z. *Z. Anorg. Allg. Chem.* **1967**, *349*, 113.
(53) Nakamura, M.; Kimizuka, N.; Mohri, T. *J. Solid State Chem.* **1990**, *86*, 16.
(54) Schinzer, C.; Heyd, F.; Matar, S. F. *J. Mater. Chem.* **1999**, *9*, 1569.
(55) Li, C. F.; Bando, Y.; Nakamura, M.; Onoda, M.; Kimizuka, N. *J. Solid State Chem.* **1998**, *139*, 347.
(56) Dupont, L.; Maugy, C.; Naghavi, N.; Guery, C.; Tarascon, J.-M. *J. Solid State Chem.* **2001**, *158*, 119.
(57) Yan, Y.; Wei, S.-H.; Al-Jassim, M. *Appl. Phys. Lett.* **2007**, *90*, 261904.
(58) Da-Silva, J. L.; Yan, Y.; Wei, S.-H. *Phys. Rev. Lett.* **2008**, *100*, 255501.
(59) Uchida, N.; Bando, Y.; Nakamura, M.; Kimizuka, N. *J. Electron Microsc.* **1994**, *43*, 146.
(60) Li, C.; Bando, Y.; Nakamura, M.; Kimizuka, N. *Micron* **2000**, *31*, 543.
(61) Minami, T.; Kakumu, T.; Takata, S. *J. Vac. Sci. Technol. A* **1996**, *14*, 1704.
(62) Kaga, H.; Asahi, R.; Tani, T. *Jpn. J. Appl. Phys.* **2004**, *43*, 3540.
(63) Maugy, C.; Dupont, L.; Naghavi, N.; Guery, C.; Tarascon, J.-M. *J. Phys. Chem. Solids* **2001**, *62*, 1375.
(64) Gonzalez, G. B.; Okasinki, J. S.; Mason, T. O.; Buslaps, T.; Honkimaki, V. *J. Appl. Phys.* **2008**, *104*, 043520.
(65) Nadaud, N.; Lequeux, N.; Nanot, M.; Jove, J.; Roisnel, T. *J. Solid State Chem.* **1998**, *135*, 140.
(66) Minami, T.; Kakumu, T.; Shimokawa, K.; Takata, S. *Thin Solid Films* **1998**, *317*, 318.
(67) O'Neil, D. H.; Kuznetsov, V.; Jacobs, R.; Jones, M. O.; Edwards, P. P. *Mater. Res. Soc. Symp. Proc.* **2008**, *1102*, LL01.
(68) Ni, J.; Yan, H.; Wang, A.; Yang, Y.; Stern, C.; Metz, A. W.; Jin, S.; Wang, L.; Marks, T.; Ireland, J. R.; Kannewurf, C. R. *J. Am. Chem. Soc.* **2005**, *127*, 5613.
(69) Metz, A. W.; Ireland, J. R.; Zheng, J.-G.; Lobo, R. P. S. M.; Yang, Y.; Ni, J.; Stern, C. L.; Dravid, V. P.; Bontemps, N.; Kannewurf, C. R.; Poeppelmeier, K. R.; Marks, T. J. *J. Am. Chem. Soc.* **2004**, *126*, 8477.
(70) Cui, J.; Wang, A.; Edleman, N. L.; Ni, J.; Lee, P.; Armstrong, N. R.; Marks, T. J. *Adv. Mater.* **2001**, *13*, 1476.
(71) Wang, A.; Edleman, N. L.; Babcock, J. R.; Marks, T. J.; Lane, M. A.; Brazis, P. W.; Kannewurf, C. R. *Mater. Res. Soc. Symp. Proc.* **2000**, *607*, 345.
(72) Minami, T. *J. Vac. Sci. Technol. A* **1999**, *17*, 1765.
(73) Naghavi, N.; Marcel, C.; Dupont, L.; Guery, C.; Maugy, C.; Tarascon, J. M. *Thin Solid Films* **2002**, *429*, 160.
(74) Minami, T.; Yamamoto, T.; Toda, Y.; Miyata, T. *Thin Solid Films* **2000**, *373*, 189.
(75) Moriga, T.; Okamoto, T.; Hiruta, K.; Fujiwara, A.; Nakabayashi, I.; Tominaga, K. *J. Solid State Chem.* **2000**, *155*, 312.
(76) Mohamed, H. A. *J. Phys. D: Appl. Phys.* **2007**, *40*, 4234.
(77) Chae, G. S. *Jpn. J. Appl. Phys.* **2001**, *40*, 1282.
(78) Mohamed, H. A. *J. Phys. D: Appl. Phys.* **2007**, *40*, 4234.
(79) Zhang, M.; Buchholz, D. B.; Xie, S. J.; Chang, R. P. H. *J. Cryst. Growth* **2007**, *308*, 376.
(80) Sohn, S.-Y.; Kim, H.-M.; Park, S.-H.; Kim, J.-J. *J. Korean Phys. Soc.* **2004**, *45*, S732.
(81) Bae, J.-H.; Moon, J.-M.; Jeong, S. W.; Kim, J.-J.; Kang, J.-W.; Kim, D.-G.; Kim, J.-K.; Park, J.-W.; Kim, H.-K. *J. Electrochem. Soc.* **2008**, *155*, J1.
(82) Ow-Yang, C. W.; Yeom, H.-y.; Paine, D. C. *Thin Solid Films* **2008**, *516*, 3105.
(83) Liu, D.-S.; Sheu, C.-S.; Lee, C.-T.; Lin, C.-H. *Thin Solid Films* **2008**, *576*, 3196.
(84) Liu, D.-S.; Lin, C.-H.; Huang, B.-W.; Wu, C.-C. *Jpn J. Appl. Phys.* **2006**, *45*, 3526.
(85) Hwang, M.-S.; Jeong, H. S.; Kim, W. M.; Seo, Y. W. *J. Vac. Sci. Technol. A* **2003**, *21*, 1399.
(86) Liu, D.-S.; Lin, C.-H.; Tsai, F.-C.; Wu, C.-C. *J. Vac. Sci. Technol. A* **2006**, *24*, 694.
(87) Naghavi, N.; Rougier, A.; Marcel, C.; Guery, C.; Leriche, J. B.; Tarascon, J. M. *Thin Solid Films* **2000**, *360*, 233.
(88) Minami, T.; Sonohara, H.; Kakumu, T.; Takata, S. *Jpn. J. Appl. Phys.* **1995**, *34*, L971.
(89) Zhang, M.; Buchholz, D. B.; Xie, S. J.; Chang, R. P. H. *J. Cryst. Growth* **2008**, *310*, 671.
(90) Reed, S. J. B. *Electron Microprobe Analysis*, 2nd ed.; Cambridge University Press: Cambridge, 1993.
(91) Kim, K.-P.; Hussain, A. M.; Hwang, D.-K.; Woo, S.-H.; Lyu, H.-K.; Baek, S.-H.; Jang, Y.; Kim, J.-H. *Jpn. J. Appl. Phys.* **2009**, *48*, 021601.

(92) Hoffman, R. L.; Norris, B. J.; Wager, J. F. *Appl. Phys. Lett.* **2003**, *82*, 733.
(93) Masuda, S.; Kitamura, K.; Okumura, Y.; Miyatake, S.; Tabata, H.; Kawai, T. *J. Appl. Phys.* **2003**, *93*, 1624.
(94) Nomura, K.; Ohta, H.; Takagi, A.; Kamiya, T.; Hirano, M.; Hosono, H. *Nature* **2004**, *432*, 488.
(95) Wager, J. F.; Keszler, D. A.; Presley, R. E. *Transparent Electronics*; Springer: New York, 2008.
(96) Nomura, K.; Kamiya, T.; Ohta, H.; Uruga, T.; Hirano, M.; Hosono, H. *Phys. Rev. B* **2007**, *75*, 035212.
(97) Nomura, K.; Kamiya, T.; Ohta, H.; Ueda, K.; Hirano, M.; Hosono, H. *Appl. Phys. Lett.* **2004**, *85*, 1993.
(98) Takagi, A.; Nomura, K.; Ohta, H.; Yanagi, H.; Kamiya, T.; Hirano, M.; Hosono, H. *Thin Solid Films* **2005**, *486*, 38.
(99) Hosono, H.; Yasukawa, M.; Kawazoe, H. *J. Non-Cryst. Solids* **1996**, *203*, 334.
(100) Noruma, K.; Kamiya, T.; Ohta, H.; Uruga, T.; Hirano, M.; Hosono, H. *Phys. Rev. B* **2007**, *75*, 035212.
(101) Robertson, J. *Phys. Status Solidi B* **2008**, *245*, 1026.
(102) Grover, M. S.; Hersh, P. A.; Chiang, H. Q.; Kettenring, E. S.; Wager, J. F.; Keszler, D. A. *J. Phys. D: Appl. Phys.* **2007**, *40*, 1335.
(103) Buchholz, D. B.; Liu, J.; Marks, T. J.; Zhang, M.; Chang, R. P. H. *Appl. Mater. Interface* **2009**, *1*, 2147.
(104) Ju, S.; Facchetti, A.; Xuan, Y.; Liu, J.; Ishikawa, F.; Ye, P.; Zhou, C.; Marks, T. J.; Janes, D. B. *Nature Nano* **2007**, *8*, 378.
(105) Ju, S.; Ishikawa, F.; Chen, P.; Chang, H.-K.; Zhou, C.; Ha, Y.-g.; Liu, J.; Faccetti, A.; Marks, T. J.; Janes, D. B. *Appl. Phys. Lett.* **2008**, *92*, 222105.
(106) Norris, B. J.; Anderson, J.; Wager, J. F.; Keszler, D. A. *J. Phys. D: Apply. Phys.* **2003**, *36*, L105.
(107) Bueno, P. R.; Varela, J. A.; Longo, E. *J. Eur. Ceram. Soc.* **2007**, *28*, 505.
(108) Zhang, G. Z.; Wang, J. F.; Chen, H. C.; Su, W. B.; Wang, W. X.; Qi, P.; Wang, C. M. *J. Mater. Sci.* **2004**, *39*, 3537.
(109) Xu, J.; Jia, X.; Lou, X.; Xi, G.; Han, J.; Gao, Q. *Sensors and Actuators B* **2007**, *120*, 694.
(110) Yu-Sheng, S.; Tian-Shu, Z. *Sens. Actuators, B* **1993**, *12*, 5.
(111) Xu, J.; Jia, X.; Lou, X.; Shen, J. *Solid-State Electron.* **2006**, *50*, 504.
(112) Wu, X.; Asher, S.; Levi, D. H.; King, D. E.; Yan, Y.; Gessert, T. A.; Sheldon, P. *J. Appl. Phys.* **2001**, *89*, 4564.
(113) Minami, T.; Takata, S.; Sato, H.; Sonohara, H. *J. Vac. Sci. Technol. A* **1995**, *13*, 1095.
(114) Minami, T.; Sonohara, H.; Takata, S.; Sato, H. *Jpn. J. Appl. Phys.* **1994**, *33*, L1693.
(115) Minami, T.; Tsukada, S.; Minamino, Y.; Miyata, T. *J. Vac. Sci. Technol. A* **2005**, *23*, 1128.
(116) Hayashi, Y.; Kondo, K.; Murai, K.; Moriga, T.; Nakabayashi, I.; Fukumoto, H.; Tominaga, K. *Vacuum* **2004**, *74*, 607.
(117) Moriga, T.; Hayashi, Y.; Kondo, K.; Nishimura, Y.; Murai, K.-i.; Nakabayashi, I.; Fukumoto, H.; Tominaga, K. *J. Vac. Sci. Technol. A* **2004**, *22*, 1705.
(118) Perkins, J. D.; Cueto, J. A. d.; Alleman, J. L.; Warmsingh, C.; Keyes, B. M.; Gedvilas, L. M.; Parilla, P. A.; Li, X.; To, B.; Readey, D. W.; Hest, M. V.; Ginley, D. S. *Conf. Rec. IEEE Photovoltaic Spec. Conf.* **2002**, *29*, 1126.
(119) Perkins, J. D.; Cueto, J. A. d.; Alleman, J. L.; Warmsingh, C.; Keyes, B. M.; Gedvilas, L. M.; Parilla, P. A.; To, B.; Readey, D. W.; Ginley, D. S. *Thin Solid Films* **2002**, *411*, 152.
(120) Young, D. L.; Williamson, D. L.; Coutts, T. J. *J. Appl. Phys.* **2002**, *91*, 1464.
(121) Enoki, H.; Nakayama, T.; Echigoya, J. *Phys. Status Solidi A* **1992**, *129*, 181.
(122) Cetinorgu, E.; Goldsmith, S.; Barkay, Z.; Boxman, R. L. *J. Phys. D: Appl. Phys.* **2006**, *39*, 5245.
(123) Kurz, A.; Aegerter, M. A. *J. Sol-Gel Sci. Technol.* **2004**, *31*, 267.
(124) Satoh, K.; Kakehi, Y.; Okamoto, A.; Murakami, S.; Uratani, F.; Yotsuya, T. *Jpn. J. Appl. Phys.* **2005**, *44*, L34.
(125) Bagheri-Mohagheghi, M.-M.; Shokooh-Saremi, M. *Thin Solid Films* **2003**, *441*, 238.
(126) Qiu, C. X.; Shih, I. *Sol. Energy Mater. Sol. Cells* **1986**, *13*, 75.
(127) Wu, X.; Coutts, T. J.; Mulligan, W. P. *J. Vac. Sci. Technol. A* **1997**, *15*, 1057.
(128) Ko, J. H.; Kim, I. H.; Kim, D.; Lee, K. S.; Lee, T. S.; Cheong, B.; Kim, W. M. *Appl. Surf. Sci.* **2007**, *253*, 7398.
(129) Kovacheva, D.; Petrov, K. *Solid State Ionics* **1998**, *109*, 327.
(130) Inaguma, Y.; Yoshida, M.; Katsumata, T. *J. Am. Chem. Soc.* **2008**, *130*, 6704.
(131) Son, J. Y.; Lee, G.; Jo, M.-H.; Kim, H.; Jang, H. M.; Shin, Y.-H. *J. Am. Chem. Soc.* **2009**, *131*, 8386.
(132) Ko, J. H.; Kim, I. H.; Kim, D.; Lee, K. S.; Lee, T. S.; Jeong, J.-H.; Cheong, B.; Baik, Y. J.; Kim, W. M. *Thin Solid Films* **2006**, *494*, 42.
(133) Chiang, H. Q.; Wager, J. F.; Hoffman, R. L.; Jeong, J.; Keszler, D. A. *Appl. Phys. Lett.* **2005**, *86*, 013503.
(134) Park, S. K.; Kim, Y.-H.; Kim, H.-S.; Han, J.-I. *Electrochem. Solid-State Lett.* **2009**, *12*, H256.
(135) Jeong, Y.; Song, K.; Kim, D.; Koo, C. Y.; Moon, J. *J. Electrochem. Soc.* **2009**, *156*, H808.
(136) Riedl, T.; Gorrn, P.; Kowalsky, W. *J. Display Technol.* **2009**, *5*, 501.
(137) Chang, Y.-J.; Lee, D.-H.; Herman, G. S.; Chang, C.-H. *Electrochem. Solid-State Lett.* **2007**, *10*, H135.
(138) Hong, D.; Chiang, H. Q.; Presley, R. E.; Dehuff, N. L.; Bender, J. P.; Park, C.-H.; Wager, J. F.; Keszler, D. A. *Thin Solid Films* **2006**, *515*, 2717.
(139) Philips, J. M.; Cava, R. J.; Thomas, G. A.; Carter, S. A.; Kwo, J.; Siegrist, T.; Krajewski, J. J.; Marshall, J. H.; W. F. Peck, J.; Rapkine, D. H. *Appl. Phys. Lett.* **1995**, *67*, 2246–2248.